Research Article | Vol. 12, No. 7 / 1 Jul 2022 / Optical Materials Express 2886
Optical Materials EXPRESS

Femtosecond laser-shockwave induced densification in fused silica

ARUNKRISHNAN RADHAKRISHNAN,* JULIEN GATEAU, PIETER VLUGTER, AND YVES BELLOUARD

Galatea Lab, STI/IEM, Ecole Polytechnique Fédérale de Lausanne (EPFL), Rue de la Maladière, 71b, Neuchâtel CH-2002, Switzerland
arunkrishnan.radhakrishnan@epfl.ch

Abstract: A tightly focused femtosecond laser-beam in the non-ablative regime can induce a shockwave sufficiently intense to reach local pressures in the giga-Pascal range or more. In a single beam configuration, the location of the highest-pressure zone is nested within the laser-focus zone, making it difficult to differentiate the effect of the shockwave pressure from photo-induced and plasma relaxation effects. To circumvent this difficulty, we consider two spatially separated focused beams individually acting as quasi-simultaneous pressure-wave emitters. The zone in between the two laser beams where both shockwaves superpose forms a region of extreme pressure range, physically separated from the regions where the plasma formed. Here, we present a detailed material investigation of pressured-induced densification in fused silica occurring in between the foci of two laser beams. The method used is generic and can be implemented in a variety of transparent substrates for high-pressure physics studies. Unlike classical methods, such as the use of diamond anvils, it potentially offers a means to create arbitrary patterns of laser-induced high-pressure impacted zones by scanning the two beams across the specimen volume.

1. Introduction

In nature, high-pressure phases of silica are found in meteorite craters resulting from high-velocity impacts [1]. Studying these phases in a laboratory setting remains a tedious task, as it requires high-pressure generation, from tens of giga-pascal (GPa) to tera-pascal (TPa) levels. While diamond anvil cells (DAC) are commonly used for the laboratory-scale high-pressure generation, it suffers from intrinsic limitations of volume and processing time restrictions [2,3].

Due to the extreme brevity of the energy deposition and the rapid expansion of the plasma that results in a strong pressure wave emission [4–9], ultrafast laser interaction with dielectrics creates the conditions for locally achieving pressure levels in the TPa levels, as reported in sapphire and fused silica using single spot experiments [10–13]. However, the high-pressure zone is nested in the laser-affected zone, making it challenging to differentiate photo-induced from pressure-only effects, as the material is not exclusively subjected to intense pressure waves, but also to the direct outcome related to plasma generated at the laser spot.

To circumvent this difficulty and effectively separate high-pressure zones from regions under direct laser-exposure; one method consists of using two spatially separated femtosecond laser pulses (as reported in the work of Hayasaki *et al.* [14]). There, two pulses act as quasi-simultaneous emitters of pressure waves that interfere with one another, leading to higher-pressure zones located effectively outside the volume where non-linear absorption took place, but rather in the region where the two pressure waves superposed, i.e. in between the two laser foci. This type of focusing have been used for laser shockwave cleaning (LSC) of silicon wafers [15], to understand the nature of weak shock wave interactions in water [16] and for multi-spot laser ablation studies [17] using ultrafast lasers.

#462915 https://doi.org/10.1364/OME.462915
Journal © 2022 Received 3 May 2022; revised 12 Jun 2022; accepted 13 Jun 2022; published 30 Jun 2022

Optical Materials EXPRESS

The shockwave emitted during the laser plasma rapid expansion and collapse, propagates longitudinally from the laser-propagation axis with an initial velocity, faster than the sound wave velocity in the material (5.9×10^3 m/s for silica), but decays within micron distances into acoustic waves [18]. In [14], the two-beam method was applied to borosilicate glass and with a spatial separation of the two foci leading to an acoustic wave regimes. Based on phase retardance measurements, transient and permanent densification of glass were reported away from the irradiation location and interpreted as the result of acoustical interaction of intense transverse and longitudinal sound waves [14].

This non-contact method offers an alternative to classical methods used to investigate the high-pressure phase in materials as there is no direct mechanical interaction to generate the high-pressure, like in diamond-anvil methods, but rather, laser foci that act as pressure sources. Here, we investigate further the effect of double-beams exposure, specifically in the regime where shockwave regime still prevails and for a material, fused silica, that can be effectively densified and that has a variety of high-pressure polymorphs. Furthermore, we focus our study on the effect on the material structure changes that we investigate using Raman spectroscopy, and for which, we effectively quantify the amount of volume changes achieved using a micro-mechanical method based on cantilevers [19].

2. Experimental setup

2.1. Optical setup and methodology

The experimental setup is shown in Fig. 2(a). A femtosecond laser (s-Pulse from Amplitude) delivering 150 fs pulses with a center wavelength of 1030 nm at a pulse repetition rate of 100 kHz is focused inside a 1 mm thick fused silica substrate (Corning 7980 OF). The laser beam is split into two beams of equal energy that are temporally and spatially separated by a varying time delay (Δt) and beam gap (Δx), respectively. The two beams are focused with the same objective (OptoSigma, NA 0.4) yielding an approximate optical spot-diameter of 1.8 μm at $1/e^2$ at 1030 nm. The effective separation between the regions where the two plasmas were located (evidenced by the presence of nanogratings) is effectively measured using scanning electron microscopy, which provides a much more accurate methods than classical optical means.

A low-energy second harmonics probe pulse (λ_{probe} = 515 nm), generated in a Beta Barium Borate (BBO) crystal, is used to precisely control the time delay between the two incoming beams, with a resolution down to tens of femtoseconds between the pump and probe signals, by visually observing the effect of the plasma formation on a standard CMOS camera placed above the focusing objective. The spatial and temporal gaps between the two machining beams are calibrated by optimizing the interference fringe pattern of the two beams and further refined by measuring the distance between laser-affected zones as observed in SEM images of polished cross-section of laser-written lines. In this set of experiments, we were able to vary the distance between laser-affected zones from 480 nm to 2 microns and the time delay from zero to 66 ps by adjusting the linear translating (LTS1) and pump delay stages respectively with a temporal resolution of 66 fs. The two beams were temporally separated enough to avoid the photon coupling between the two pulses. The laser-exposure occurred in the bulk of the material at a distance of 20 microns from the surface.

Optical Materials EXPRESS

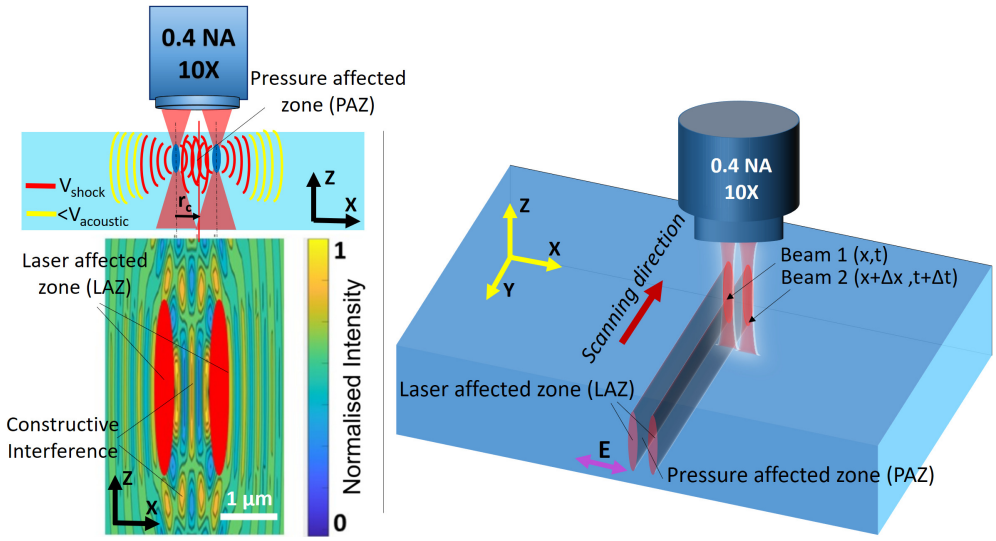

Fig. 1. Left: Double-beam femtosecond laser bulk exposure: schematic view of the cross-section (top left) and constructive wave interference pattern shown in the acoustic regime for the illustrative purpose (bottom left). The two laser beams emit shock waves that add up in between the beams location. These decaying shock waves interfere constructively between the two foci. Right: Continuous line-patterns scanning principle. The double-beam exposure can be applied anywhere through the specimens. The two pulses are temporally separated by the pulse length to prevent optical interferences, yet for a duration order of magnitude shorter than the time scale of shockwave emission to consider the two events as instantaneous at the time scale of stress waves propagation. The electric field vector E is perpendicular to the direction of writing.

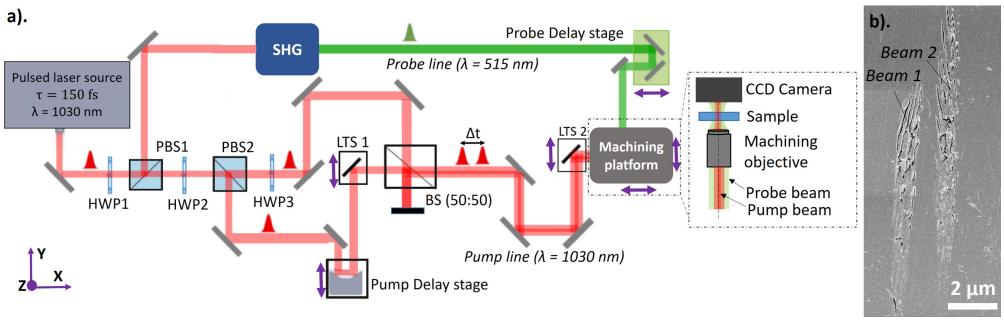

Fig. 2. a. Optical layout of the double-beam experiment setup. A part of the incoming laser beam is converted into a frequency-doubled probe beam using second harmonics generation (SHG) with a BBO crystal. The beam gap and the temporal delay are adjusted by a linear translation stage (LTS 1) and a pump delay line, respectively. The front schematic sketch of the machining platform is shown in the right inset. (BSP: Beam splitter polarizer cube, HWP: Half wave plate, LTS: Linear translation stage, BBO: beta barium borate crystal); b. SEM image of the cross-section of the machined sample. Here the beams are having a gap of approximately one micron.

Optical Materials EXPRESS

3. Results and discussions

3.1. Densification measurements

The cross-section of the line patterns produced by the double beams were analyzed using micro-Raman spectroscopy (Renishaw InVia confocal Raman spectroscope using a 100X objective, spot size < 1μm). Here, we choose 405 nm as the excitation laser wavelength for stimulated Raman emission to prevent fluorescence excitation of laser-induced defects that could shadow other Raman peaks. Each measurement point in the scan was obtained with a laser power of 4.6 mW and a total exposure time of 20 seconds. Figure 3 represents the Raman measurements taken outside and within the laser-modified zones, polished along their cross-section oriented towards the optical laser propagation axis. In this illustration, the beams are spatially separated by a distance of 1.2 microns and temporally by a time delay of 240 fs. The data are presented for three distinct zones, namely, the zone outside the laser affected zones (labeled 'Zone O'), the zone located along the laser exposed pattern ('Zone L'), and finally, the zone in between the two laser affected zones ('Zone M'), which is the zone where the two shockwaves are superposed. All Raman spectra are normalized with respect to the ω_4 band, related to the Si-O stretching motion, which is considered less affected, by structural changes, such as rings densification. On the one hand, 'Zone O', located one micron away from the laser exposed zone, shows no visible difference in the Raman spectra compared to a reference (as seen in Fig. 3 (left)) along all measurement points, while the pressure affected zone (zone M) was found to have a modification in the region of shock superposition, particularly among the points M1 and M2 as shown in Fig. 3 (right). At these points, we observed a rise in the D_1 (495 cm^{-1}) and D_2 (605 cm^{-1}) peaks that correspond to in-phase breathing modes of oxygen atoms in 4 and 3-members rings respectively [20–22], along with a shift of the peaks towards higher wavenumbers (Fig. 3(b)), which accounts for the reduction in bond angle of the silica lattice [23,24] in Zone M.

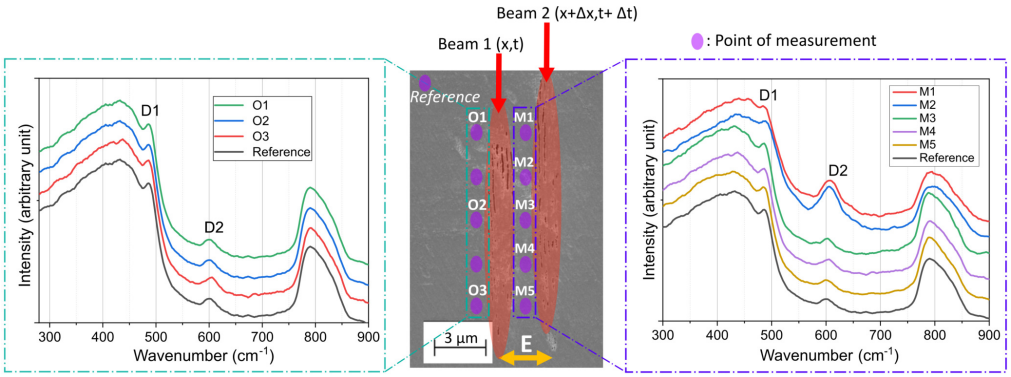

Fig. 3. Comparison between Raman spectra taken in the zone outside the laser affected zone (denoted by O) and the zone in between (denoted by M) the laser affected zones; Middle/ Microscopic image of the point of measurement along the cross-section of the machined lines, where E is the electric field vector of both the beams and is oriented normal to the scanning direction; Left & right / Raman spectra of the zones outside the laser affected zone (denoted by O), and along the pressure affected zone in the middle of the beams (M), respectively. We can note there is a shift of the D_1-peak and an increase in D_2-peak indicating densification in the zone between the beams.

These relative changes, combined in Fig. 4, point towards the densification of the material in between the two laser-affected zones. As this zone is located outside the laser-exposed zone, we attribute this densification to the effect of shock wave superposition. By comparing these variations in spectra to the compressive hydrostatic loading experiments reported elsewhere, we

Optical Materials EXPRESS

estimate a pressure development of about 13-14 GPa by estimating the Raman parameter σ and the main band shift as mentioned in [25,26] (see Fig. 4(a)). The Raman parameter σ is defined as the Raman shift value that provides the average estimate of the densification correlating the area of the main band. It is determined by subtracting the baseline followed by calculating the Raman parameter mathematically from the equation given below [25],

$$\frac{\int_{\omega 1}^{\sigma} I_{raman}(\omega)\, d\omega}{\int_{\omega 1}^{\omega 2} I_{raman}(\omega)\, d\omega} = \frac{1}{2}. \tag{1}$$

In our estimate we took ω_1 and ω_2 as 200 and 700 cm^{-1} respectively. It can be noted that Raman frequency both shift toward higher wavelengths upon densification [25]. While this method gives a first estimate of the pressure, it assumes a hydrostatic loading case, which differs from our conditions and, in fact, underestimates the actual pressure. In our case, the modifications are obtained as a result of dynamic shock waves superposition. Based on silica shockwave densification studies [27], we estimate a pressure development of about 25-30 GPa by correlating the shift and rise of the D_2 peak, as shown in Fig. 4(c). The latter study provides higher pressure since we have the shock superposition just over a limited period of time in the case of dynamic loading conditions. To explain why points M3-M5 do not show the same behavior as points M1-M2, we note that there was a shift in one of the beams along the optical propagation axis direction due to alignment errors, which may have resulted in uneven pressure distribution. Another possible explanation while examining Raman spectra *inside* laser affected zones, is the anisotropic pressure distribution in these zones. These two observations may explain the lack of evidence for densified zones in between the tails of laser affected zones.

3.1.1. Modification along the laser affected zone

The 'Zone L', located in the left laser affected zone, exhibits clear modifications in the Raman spectra, which is expected based on previously reported data [28,29] as shown in Fig. 5 (left), when compared to the pressure affected zone shown in the Fig. 5 (right). Measurement points near the head of the laser affected zone show more densification in the Raman spectra than the ones measured near the tail of the laser affected zone (LAZ). The tear-shaped geometry of the LAZ and the reduced intensity near the trailing edge [30,31] may explain this effect. We observed a density of 2.35 g/cm^3 while comparing the D_2 intensity and FWHM of the main band as mentioned in [32].

It was also found that the densification *inside* the LAZ is higher than the densification due to homogeneous modification, a densification exposure regime found at shorter pulse duration, and lower pulse energy [33]. This result may sound counter-intuitive at first. In the regime where nanogratings form, there is a net volume expansion due to the presence of nanopores [19,34], while densification would suggest the opposite behavior. To raise this apparent contradiction, one needs to consider that the Raman observations are related to the *silica* material present in a *composite* structure, consisting of alternating sponge-like layers (consisting of a scaffold of silica with nanopores) and interstitial pressurized plain silica nanoplanes [35]. Apart from the fact that the scaffold may have itself a denser silica structure than the bulk material, the interstitial nanoplanes that are squeezed in between volume-expanding porous layers, densify. This observation is in good agreement with recent findings related to abnormal thermomechanical properties of laser modified silica [36,37] and can be correlated with previous form birefringence observations [38].

Using the same method proposed by [25] and used for the first estimate of the pressure *in between* the beams, we estimate a pressure approaching 16 GPa (see Fig. 6). This estimate is based on the assumption of hydrostatic pressure conditions and, therefore, most likely underestimates what the real pressure was, as the loading case is present for a short duration and may liken the one

Optical Materials EXPRESS

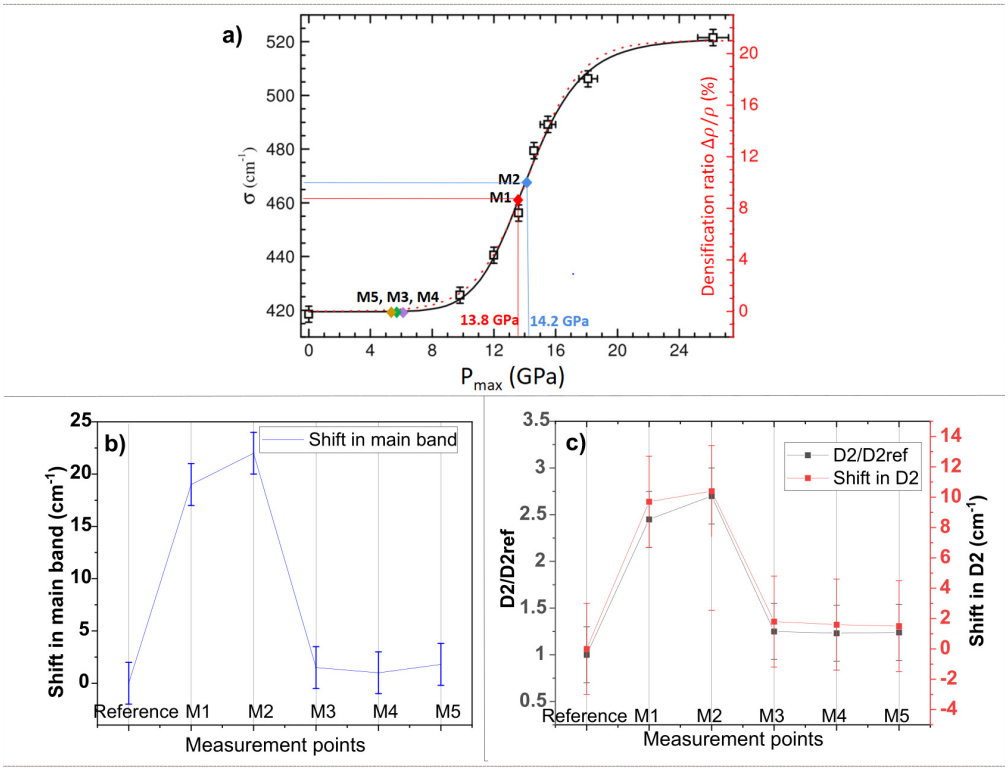

Fig. 4. a. The Raman parameter σ as a function of the maximum pressure reached P_{max} as adapted from [25] and the data from pressure affected zones was used to estimate the P_{max} after double laser beam machining; b. The shift of the main band along the pressure affected zone in the middle of the beams (M); c. The shift of D_2 peak and the ratio of the D_2 peak with respect to the D_2 reference peaks plotted along the pressure affected zone (M).

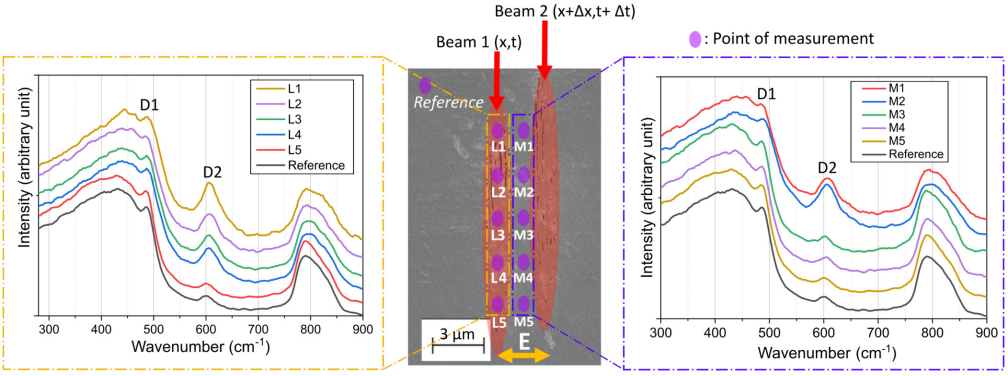

Fig. 5. Comparison between Raman spectra taken in the zone along the laser affected zone (measurement points labelled L) (left) and the ones taken in the zone in between the laser affected zones (measurement points labelled M) (right); Middle: SEM microscope image with the location of the Raman measurement points (Zone L and M) and the laser-affected zones highlighted.

Optical Materials EXPRESS

of a shock wave. However, as we are, unlike in the previous case, *within* the laser-affected zone, and hence in the zone where the plasma formed (that yielded to the formation of nanogratings), it remains speculative to truly assess what the pressure conditions as we lack an equation of state for the matter under such extreme transient conditions. We also further noticed that the modification obtained inside the LAZ is independent of the shock wave emitted by a neighboring LAZ, as identical Raman spectra were obtained inside LAZ when the beams were far apart *both* spatially and temporally.

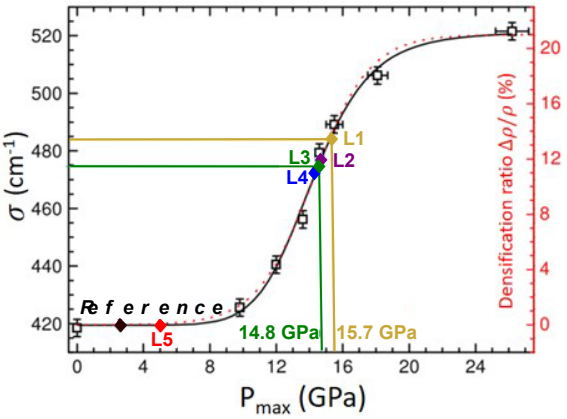

Fig. 6. The Raman parameter σ as a function of the maximum pressure reached P_{max} as adapted from [25]. The data inside the laser affected zones (Zone L) are superimposed to estimate P_{max} in our specific case.

3.2. *Effect of beam gap and time delay in the pressure affected zone*

To further investigate the densification effect occurring in between focal zones, dual-line patterns were drawn in the fused silica substrates for varying beam gap (Δx) and time delay (Δt). The patterns were systematically analyzed using Raman spectroscopy following the same method than described in the previous paragraph, and we used the ratio D_2/D_{2ref} as an indirect metric of the densification. Figure 7 denotes the densification with varying beam gap, but for a constant time delay of 240 fs. The data corresponds to point M2 in Zone M, as indicated in Fig. 3 (middle), a point where the maximum densification was obtained. The maximum densification peaks between 480 nm and 1.2 microns, which indicates the expected decay of the pressure waves [10,39] after a specific critical radius r_c as shown in Fig. 1 (left) where the shock waves decays to acoustic waves. Beyond r_c, the pressure superposition is not sufficient to induce permanent densification. Figure 7(b) shows a contour plot for D_2/D_{2ref} contrast for varying time delays for various beam gaps. By taking into account the supersonic velocity approximation from Hugoniot data of fused silica [40,41], we could suppose that above 6.6 ps, the superposition occurs near or beyond the boundary of the trailing beam's laser affected zone. Further, for lines exposed with 'infinite time delay', i.e., lines written sequentially one after the other, masking each beam sequentially, we did not achieve much higher densification parameters than the beams written without masking each other. The map suggests that maximum densification is obtained when the beam gap is less than one micron and when the beam delay is less than 500 fs. This window of parameters can be used for generating a localized densified zone between two laser-affected zones, thereby having a varying refractive index regime for instance. Note that we could not observe an obvious variation in residual pressure, while changing the polarization orientation of the laser beams. The process seems to be polarization-orientation independent.

Optical Materials EXPRESS

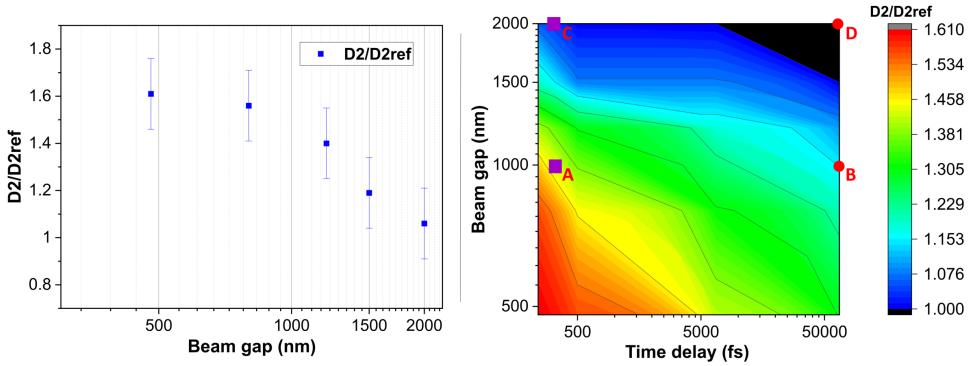

Fig. 7. a. Comparison plot between D_2/D_{2ref} ratio and beam gap (Δx) for a fixed time delay (240 fs); b. Contour map between beam gap and time delay in terms of the extent of the rise in D_2 peak.

3.3. *Volume variation measurement in double beam machined fused silica specimen as evidence of densification*

To complement Raman data and to independently confirm the presence of densification, we use a method based on deflection of micro-cantilevers [19,34] to investigate localized volume variations resulting from the double-beam femtosecond laser exposure inside the bulk of silica. The working principle is depicted in Fig. 8, where a transparent cantilever is exposed to a laser beam closer to the anchoring point and a few microns below the top surface. Here the laser exposed part (red zones) and the unexposed region constitute a bimorph composite structure. Volume expansion in the laser affected zones of individual beams will bend down the bimorph element while the densification or volume reduction in the bimorph element shall result in bending in the opposite direction. This method is highly sensitive and has also been used for investigating the coefficient of thermal expansion changes after laser exposure [37]. This experimental technique is adapted to the double beam exposure, where a series of twin lines (red zones in Fig. 8) with a definite spacing l_s, are written along the upper part of the cantilever and towards the anchoring joint. This results in a bimorph composite with an amplified displacement (δ) in the transparent glass cantilever. Here, we exposed various cantilevers with varying time delays and beam gaps. On assuming laser affected zones as a continuously and homogeneously modified layer on a bulk-unmodified substrate, we calculate the average stress (σ_{xx}) and average strain ϵ_{avg} in the laser affected zones from the measured cantilever deflection using Stoney's equation [19]. The results are shown in Fig. 9 for four representative exposure conditions (labeled A to D) and reported in Fig. 7(b). The difference in the average stress (117 MPa) between the point A and C is in agreement with the formation of a high density amorphous phase (HDA) at conditions of point A that corresponds to the highest density case in between the laser affected zones, as suggested from the Raman observations, phase [42,43]. Indeed, this zone results in a reduced cantilever deflection due to the volume compaction found in between laser-affected zones, which in turn leads to a decrease in average stress.

Further, mathematical modeling was done assuming a uniform stress along the laser affected zones, to estimate the strain along an arc oriented towards axis x. The contributions of the different zones to the average strain are given in the equation below, where ϵ_l, ϵ_s, and ϵ_{sw} are strain in the laser affected volume (Zone L), in between the two set of lines (Zone O) and the zone where the shockwaves superimpose (Zone M), respectively. The strain in zone O is due to the constant stress (σ_{xx}) in the LAZ and it is defined as,

$$\epsilon_s = \frac{\sigma_{xx}}{E} \tag{2}$$

Optical Materials EXPRESS

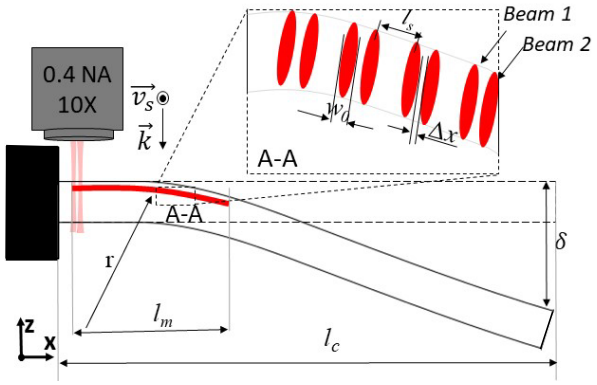

Fig. 8. Schematic cross section of a cantilever, used with double-beam laser exposure conditions. In this illustration, the cantilever bends with a radius r, and results in an overall deflection δ, due to volume expansion. In the magnified rectangle A-A, the red ellipses represent the line cross-section, with individual width w_0 and separated by a beam gap Δx.

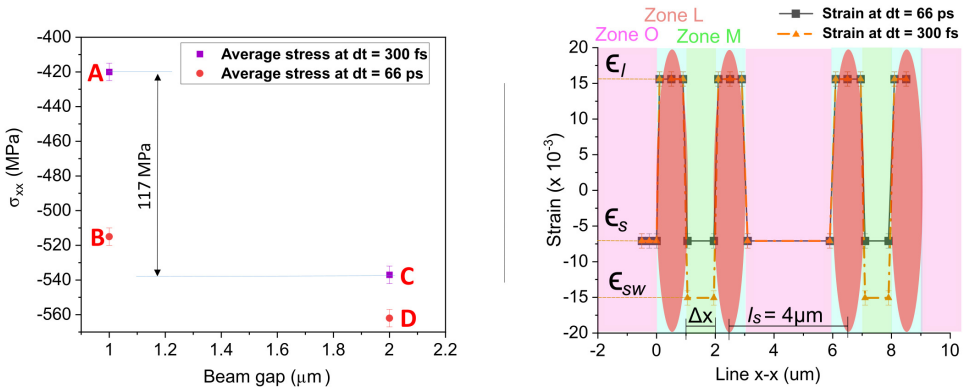

Fig. 9. a. Average stress for selected time delays (dt) and beam gaps (A-D). Exposure conditions for these four cases are shown in Fig. 4; b. Strain profile along an arc x-x for a beam gap of 1 micron, as shown in the inset of Fig. 8 (rectangle A-A).

where E is the young modulus of the material. The average stress of the cantilever shall be written as,

$$\epsilon_{\text{avg}} = \epsilon_l V_l + \epsilon_s V_s + \epsilon_{sw} V_{sw} \tag{3}$$

where V_l, V_s, and V_{sw} are the respective volume fractions and they are defined as, $V_l = 2w_0/l_s$, $V_s = 1 - 2w_0/l_s$ and $V_{sw} = \Delta X/l_s$. Here, we assume there is no shock-wave contribution when the laser beams are sufficiently temporarily separated i.e. $\epsilon_{sw} = 0$. On solving the average stress equation for the two extreme cases as shown in Fig. 7(b), where there is limited contribution and maximum contribution from the shockwave, in the case of a time delay of 66 ps and 300 fs respectively, we obtain ϵ_l and ϵ_{sw}. The pictorial representation of strain distribution is given in Fig. 9(b). Though we may note a strain of 10% from the Raman shift of D2 as mentioned in [27]; It should also be noted that the peak densification obtained at point M2 as in Fig. 4 is diluted for these measurement as we estimate the average strain from the cantilever deflection. We shall note how the strain varies along the section and the change in the strain rate in between the laser-affected zone, clearly emphasizing the effect of a remnant strain due to the shockwave (ϵ_{sw}), and hence the presence of a shock-induced densified zone. The strain obtained in our case

Optical Materials EXPRESS

is an average stress, and hence it is logical to have a lower value compared to the densification ratio obtained in shockwave experiments for which the entire element is subjected to uniform shock loading [27].

3.4. Effect of dual-beam exposure parameters on chemical etching selectivity

It is known that femtosecond-laser affects the etching rate [44,45], which itself depends on stress, density and structure of the materials. Various etchants are used for etching the laser affected zones to obtain high aspect ratios which can be used in micro-mechanical applications [46–50]. It has been known that the double beam machining enhances the etching rate [45]. To understand the effect of dual-beam exposure on etching rate, a series of lines are drawn in the bulk of a fused silica substrate, as shown in Fig. 10(a). After exposure, the substrate is cut using a diamond wire-saw, along section B-B as in Fig. 10(b), and later submerged in 2.5% HF bath for a preferential etching of 4.5 hours. The effect on the etching rate of varying time delays and beam gaps is plotted as shown in Fig. 10(c). The contour plot suggests a correlation with the densification experiments and confirms other experiments reported in Agarwal *et al.* [51]. The increased etching rate is attributed to the densification due to the compressive loading by the shock waves that resulted in compressive stress similar to mechanical, hydrostatic loading [51].

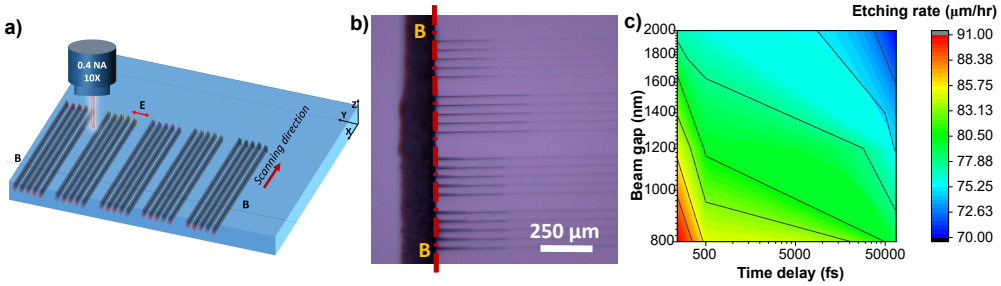

Fig. 10. a. Schematic layout for the etching experiment. The sample is divided into several patterns, where each patch has a specific time delay and beam gap; b. The bright-field microscope top view image of selected patterns of the etched sample; c. Contour plot of etching rate with varying time delay and beam gap.

4. Conclusion

Using near-simultaneous adjacent but *non-overlapping* femtosecond laser beams, we have observed that one can obtain permanent localized densification *in between* laser affected zones and this while while preserving the integrity of the material. Evidence of localized densification in between the two laser beams was obtained using Raman spectroscopy in the zone between laser affected zones and confirmed with a non-optical micro-mechanical method based on cantilever deflection [19,34]. We interpret this result as the consequence of shockwave superposition. Interestingly, this shock-wave induced densification observation is correlated with an selective etching enhancement data effect that is in agreement with density-induced etching enhancement, reported in substrate under compressive loading condition [51]. In conclusion, the exposure method illustrated here offers a means for studying the state of matter under high-velocity impact stress without the need for a direct contact method, like using a diamond anvil. Although the pressure obtained remained modest with our setup configuration (a few tens of GPa), this approach illustrates a possible pathway toward non-contact laser-induced high-pressure studies, where pressured-zone are separated from laser exposed zones.

Funding. Schweizerischer Nationalfonds zur Förderung der Wissenschaftlichen Forschung (FNS 200021 169681); European Research Council (ERC-2012-StG-307442).

Optical Materials EXPRESS

Acknowledgments. We thank Prof. Céline Hebert and Dr. Farhang Nabiei of the Physics Department, EPFL, and Ruben Ricca, Dr. Margarita Lesik Galatea lab, EPFL, for the fruitful discussions along with helping out with the cantilever experiment and formatting the draft. We would also like to thank Dr. Richard Gaal and Dr. Arnoud Magrez of the Earth and planetary science department and Crystallographic facility, EPFL, respectively, for the training with the Raman spectroscope. In this work, AR performed the material exposure and related analysis experimental work. JG implemented the optical setup. PV contributed to the cantilever deflection experiments and the micro-mechanical analysis of the laser-induced effect. YB designed and supervised the research. All the authors contributed to the initial manuscript writing and subsequent revisions.

Disclosures. The authors declare no conflicts of interest.

Data availability. Data underlying the results presented in this paper are publicly available at this time but may be obtained from the authors upon request.

References

1. P. Gillet and A. E. Goresy, "Shock events in the solar system: the message from minerals in terrestrial planets and asteroids," Annu. Rev. Earth Planet. Sci. **41**(1), 257–285 (2013).
2. A. Jayaraman, "Diamond anvil cell and high-pressure physical investigations," Rev. Mod. Phys. **55**(1), 65–108 (1983).
3. P. Richet and P. Gillet, "Pressure-induced amorphization of minerals; a review," Eur. J. Mineral. **9**(5), 907–934 (1997).
4. D. Devaux, R. Fabbro, L. Tollier, and E. Bartnicki, "Generation of shock waves by laser-induced plasma in confined geometry," J. Appl. Phys. **74**(4), 2268–2273 (1993).
5. X. Zeng, X. Mao, S. S. Mao, S.-B. Wen, R. Greif, and R. E. Russo, "Laser-induced shockwave propagation from ablation in a cavity," Appl. Phys. Lett. **88**(6), 061502 (2006).
6. L. Berthe, R. Fabbro, P. Peyre, L. Tollier, and E. Bartnicki, "Shock waves from a water-confined laser-generated plasma," J. Appl. Phys. **82**(6), 2826–2832 (1997).
7. Y. Hayasaki, M. Isaka, A. Takita, and S. Juodkazis, "Time-resolved interferometry of femtosecond-laser-induced processes under tight focusing and close-to-optical breakdown inside borosilicate glass," Opt. Express **19**(7), 5725–5734 (2011).
8. K. Bergner, B. Seyfarth, K. A. Lammers, T. Ullsperger, S. Döring, M. Heinrich, M. Kumkar, D. Flamm, A. Tünnermann, and S. Nolte, "Spatio-temporal analysis of glass volume processing using ultrashort laser pulses," Appl. Opt. **57**(16), 4618 (2018).
9. M. Sakakura, M. Terazima, Y. Shimotsuma, K. Miura, and K. Hirao, "Observation of pressure wave generated by focusing a femtosecond laser pulse inside a glass," Opt. Express **15**(9), 5674–5686 (2007).
10. S. Juodkazis, K. Nishimura, S. Tanaka, H. Misawa, E. G. Gamaly, B. Luther-Davies, L. Hallo, P. Nicolai, and V. T. Tikhonchuk, "Laser-induced microexplosion confined in the bulk of a sapphire crystal: evidence of multimegabar pressures," Phys. Rev. Lett. **96**(16), 166101 (2006).
11. A. Vailionis, E. G. Gamaly, V. Mizeikis, W. Yang, A. V. Rode, and S. Juodkazis, "Evidence of superdense aluminium synthesized by ultrafast microexplosion," Nat. Commun. **2**(1), 445 (2011).
12. E. G. Gamaly, A. V. Rode, B. Luther-Davies, and V. T. Tikhonchuk, "Ablation of solids by femtosecond lasers: Ablation mechanism and ablation thresholds for metals and dielectrics," Phys. Plasmas **9**(3), 949–957 (2002).
13. S. Juodkazis, S. Kohara, Y. Ohishi, N. Hirao, A. Vailionis, V. Mizeikis, A. Saito, and A. Rode, "Structural changes in femtosecond laser modified regions inside fused silica," J. Opt. **12**(12), 124007 (2010).
14. Y. Hayasaki, M. Isaka, A. Takita, S. Hasegawa, and S. Juodkazis, "Photo-acoustic sub-micrometer modifications of glass by pair of femtosecond laser pulses," Opt. Mater. Express **2**(5), 691–699 (2012).
15. S. Zhang, Q. Yan, J. Lin, Q. Zhang, Y. Lu, J. Yao, and L. Fan, "Elimination of blind zone in nanoparticle removal on silicon wafers using a double-beam laser shockwave cleaning process," Appl. Surf. Sci. **539**, 148057 (2021).
16. M. Vreugdenhil, D. van Oosten, and J. Hernandez-Rueda, "Dynamics of femtosecond laser-induced shockwaves at a water/air interface using multiple excitation beams," Opt. Lett. **43**(20), 4899–4902 (2018).
17. T. Zhou, S. Kraft, W. Perrie, J. Schille, U. Löschner, S. Edwardson, and G. Dearden, "Backward Flux Re-Deposition Patterns during Multi-Spot Laser Ablation of Stainless Steel with Picosecond and Femtosecond Pulses in Air," Materials **14**(9), 2243 (2021).
18. E. G. Gamaly, S. Juodkazis, K. Nishimura, H. Misawa, B. Luther-Davies, L. Hallo, P. Nicolai, and V. T. Tikhonchuk, "Laser-matter interaction in the bulk of a transparent solid: Confined microexplosion and void formation," Phys. Rev. B **73**(21), 214101 (2006).
19. A. Champion and Y. Bellouard, "Direct volume variation measurements in fused silica specimens exposed to femtosecond laser," Opt. Mater. Express **2**(6), 789–798 (2012).
20. F. L. Galeener, "Band limits and the vibrational spectra of tetrahedral glasses," Phys. Rev. B **19**(8), 4292–4297 (1979).
21. F. L. Galeener, R. A. Barrio, E. Martinez, and R. J. Elliott, "Vibrational decoupling of rings in amorphous solids," Phys. Rev. Lett. **53**(25), 2429–2432 (1984).
22. F. L. Galeener and G. Lucovsky, "Longitudinal optical vibrations in glasses: GeO_2 and SiO_2," Phys. Rev. Lett. **37**(22), 1474–1478 (1976).

Optical Materials EXPRESS

23. P. N. Sen and M. F. Thorpe, "Phonons in AX_2 glasses: From molecular to band-like modes," Phys. Rev. B **15**(8), 4030–4038 (1977).
24. M. Sakakura, M. Terazima, Y. Shimotsuma, K. Miura, and K. Hirao, "Thermal and shock induced modification inside a silica glass by focused femtosecond laser pulse," J. Appl. Phys. **109**(2), 023503 (2011).
25. T. Deschamps, A. Kassir-Bodon, C. Sonneville, J. Margueritat, C. Martinet, D. de Ligny, A. Mermet, and B. Champagnon, "Permanent densification of compressed silica glass: A Raman-density calibration curve," J. Phys.: Condens. Matter **25**, 025402 (2012).
26. C. Sonneville, A. Mermet, B. Champagnon, C. Martinet, J. Margueritat, D. de Ligny, T. Deschamps, and F. Balima, "Progressive transformations of silica glass upon densification," J. Chem. Phys. **137**(12), 124505 (2012).
27. M. Okuno, B. Reynard, Y. Shimada, Y. Syono, and C. Willaime, "A Raman spectroscopic study of shock-wave densification of vitreous silica," Phys. Chem. Miner. **26**(4), 304–311 (1999).
28. Y. Bellouard, E. Barthel, A. A. Said, M. Dugan, and P. Bado, "Scanning thermal microscopy and Raman analysis of bulk fused silica exposed to low-energy femtosecond laser pulses," Opt. Express **16**(24), 19520–19534 (2008).
29. J. W. Chan, T. Huser, S. Risbud, and D. M. Krol, "Structural changes in fused silica after exposure to focused femtosecond laser pulses," Opt. Lett. **26**(21), 1726–1728 (2001).
30. F. Docchio, P. Regondi, M. R. C. Capon, and J. Mellerio, "Study of the temporal and spatial dynamics of plasmas induced in liquids by nanosecond Nd:YAG laser pulses. 1: Analysis of the plasma starting times," Appl. Opt. **27**(17), 3661–3668 (1988).
31. I. M. Burakov, N. M. Bulgakova, R. Stoian, A. Mermillod-Blondin, E. Audouard, A. Rosenfeld, A. Husakou, and I. V. Hertel, "Spatial distribution of refractive index variations induced in bulk fused silica by single ultrashort and short laser pulses," J. Appl. Phys. **101**(4), 043506 (2007).
32. Y. Wang, M. Cavillon, N. Ollier, B. Poumellec, and M. Lancry, "An overview of the thermal erasure mechanisms of femtosecond laser-induced nanogratings in silica glass," Phys. Status Solidi A **218**(12), 2100023 (2021).
33. P. Vlugter, E. Block, and Y. Bellouard, "Local tuning of fused silica thermal expansion coefficient using femtosecond laser," Phys. Rev. Mater. **3**(5), 053802 (2019).
34. Y. Bellouard, A. Champion, B. McMillen, S. Mukherjee, R. R. Thomson, C. Pépin, P. Gillet, and Y. Cheng, "Stress-state manipulation in fused silica via femtosecond laser irradiation," Optica **3**(12), 1285–1293 (2016).
35. M. Lancry, B. Poumellec, J. Canning, K. Cook, J.-C. Poulin, and F. Brisset, "Ultrafast nanoporous silica formation driven by femtosecond laser irradiation," Laser Photonics Rev. **7**(6), 953–962 (2013).
36. P. Vlugter and Y. Bellouard, "Abnormal temperature dependent elastic properties of fused silica irradiated by ultrafast lasers," Phys. Rev. Mater. **6**(3), 033602 (2022).
37. P. Vlugter and Y. Bellouard, "Elastic properties of self-organized nanogratings produced by femtosecond laser exposure of fused silica," Phys. Rev. Mater. **4**(2), 023607 (2020).
38. E. Bricchi, B. G. Klappauf, and P. G. Kazansky, "Form birefringence and negative index change created by femtosecond direct writing in transparent materials," Opt. Lett. **29**(1), 119–121 (2004).
39. Y. B. Zel'dovich and Y. P. Raizer, *Physics of Shock Waves and High-Temperature Hydrodynamic Phenomena* (Dover Publications, 2002).
40. M. Koenig, B. Faral, J. M. Boudenne, D. Batani, A. Benuzzi, and S. Bossi, "Optical smoothing techniques for shock wave generation in laser-produced plasmas," Phys. Rev. E **50**(5), R3314–R3317 (1994).
41. M. P. Desjarlais, M. D. Knudson, and K. R. Cochrane, "Extension of the Hugoniot and analytical release model of α-quartz to 0.2–3 TPa," J. Appl. Phys. **122**(3), 035903 (2017).
42. A. E. Gleason, C. A. Bolme, H. J. Lee, B. Nagler, E. Galtier, D. Milathianaki, J. Hawreliak, R. G. Kraus, J. H. Eggert, D. E. Fratanduono, G. W. Collins, R. Sandberg, W. Yang, and W. L. Mao, "Ultrafast visualization of crystallization and grain growth in shock-compressed SiO2," Nat. Commun. **6**(1), 8191 (2015).
43. A. E. Gleason, C. A. Bolme, H. J. Lee, B. Nagler, E. Galtier, R. G. Kraus, R. Sandberg, W. Yang, F. Langenhorst, and W. L. Mao, "Time-resolved diffraction of shock-released SiO_2 and diaplectic glass formation," Nat. Commun. **8**(1), 1481 (2017).
44. S. Rajesh and Y. Bellouard, "Towards fast femtosecond laser micromachining of fused silica: the effect of deposited energy," Opt. Express **18**(20), 21490–21497 (2010).
45. A. Mouskeftaras and Y. Bellouard, "Effect of the combination of femtosecond laser pulses exposure on the etching rate of fused silica in hydrofluoric acid," J. Laser Micro/Nanoeng. **13**(1), 26–30 (2018).
46. Y. Kondo, J. Qiu, T. Mitsuyu, K. Hirao, and T. Yoko, "Three-dimensional microdrilling of glass by multiphoton proces and chemical etching," Jpn. J. Appl. Phys. **38**(Part 2, No. 10A), L1146–L1148 (1999).
47. C. A. Ross, D. G. MacLachlan, D. Choudhury, and R. R. Thomson, "Optimisation of ultrafast laser assisted etching in fused silica," Opt. Express **26**(19), 24343–24356 (2018).
48. C. Hnatovsky, R. S. Taylor, E. Simova, V. R. Bhardwaj, D. M. Rayner, and P. B. Corkum, "Polarization-selective etching in femtosecond laser-assisted microfluidic channel fabrication in fused silica," Opt. Lett. **30**(14), 1867–1869 (2005).
49. Y. Bellouard, A. Said, M. Dugan, and P. Bado, "Fabrication of high-aspect ratio, micro-fluidic channels and tunnels using femtosecond laser pulses and chemical etching," Opt. Express **12**(10), 2120–2129 (2004).
50. E. Casamenti, S. Pollonghini, and Y. Bellouard, "Few pulses femtosecond laser exposure for high efficiency 3D glass micromachining," Opt. Express **29**(22), 35054 (2021).

Optical Materials EXPRESS

51. A. Agarwal and M. Tomozawa, "Correlation of silica glass properties with the infrared spectra," J. Non-Cryst. Solids **209**(1-2), 166–174 (1997).